metals

MDPI

Article

Effect of Calcium Oxide on the Crushing Strength, Reduction, and Smelting Performance of High-Chromium Vanadium–Titanium Magnetite Pellets

Gongjin Cheng [1,*], Zixian Gao [1], He Yang [1,2] and Xiangxin Xue [1,2,*]

1 School of Metallurgy, Northeastern University, Shenyang 110819, China; gaozixian1992@163.com (Z.G.); yangh@smm.neu.edu.cn (H.Y.)

2 Liaoning Key Laboratory of Recycling Science for Metallurgical Resources, Shenyang 110819, China

* Correspondence: successking123@gmail.com (G.C.); xuexx@mail.neu.edu.cn (X.X.); Tel.: +86-24-8368-4086 (G.C.); +86-24-8368-7306 (X.X.); Fax: +86-24-2390-6316 (G.C. & X.X.)

Academic Editor: Ian Baker

Received: 18 March 2017; Accepted: 17 May 2017; Published: 19 May 2017

Abstract: The effect of calcium oxide on the crushing strength, reduction, and smelting performance of high-chromium vanadium–titanium magnetite pellets (HCVTMP) was studied in this work. The main characterization methods of an electronic universal testing machine (EUTM), X-ray fluorescent (XRF), inductively-coupled plasma-atomic emission spectroscopy (ICP-AES), X-ray diffraction (XRD), and scanning electron microscope-energy disperse spectroscopy (SEM-EDS) were employed. The crushing strength was affected by the mineral phases generated during oxidative baking and the subsequently-formed pellet microstructures owing to CaO addition. The reduction and smelting properties of HCVTMP with different CaO additives were measured and characterized with different softening-melting-dripping indices. Although HCVTMP showed the highest crushing strength with CaO addition of ca. 2 wt %, more CaO addition may be needed to achieve high permeability of the furnace burdens and a good separation condition of the slag and melted iron. In the formation process of the slag and melted iron, it can be determined that CaO could have a relationship with the transformation behavior of Cr, V, and Ti to some extent, with respect to the predominant chemical composition analysis of ICP-AES and XRF. With the microscopic examination, the restraining formation of Ti(C,N) and the promoting formation of $CaTiO_3$ are in accordance with the improved melting-dripping indices, including the decrease of the maximum external static load and gas permeability, and the increase of the melting-dripping zone and dripping difficulty.

Keywords: high-chromium vanadium–titanium magnetite; calcium oxide; crushing strength; reduction and smelting

1. Introduction

Vanadium–titanium magnetite [1–5], as one kind of significant mineral resources, is rich in the valuable elements Fe, V, Ti, Cr, etc., and there are greater than 45 billion tons of these specific ores that are distributed mainly in the Ural region of Russia, the Panxi, Chengde, and Maanshan regions of China, the Bushveld region of South Africa, the Seaside region of Western Australia, the west coast of the North Island of New Zealand, Canada, America, etc. These are ordinary vanadium–titanium magnetite and high-chromium vanadium–titanium magnetite (HCVTM), according to the mass fraction of Cr_2O_3, and the determining criterion of the mass fraction is 0.3 wt % [1,3,6–8]. As it is known, great quantities of studies have been done for ordinary vanadium–titanium magnetite, while studies on high-chromium vanadium–titanium magnetite with the coarse grain size, poor quality, and complex

mineral phases and microstructures have been scarce [1,3,6–9]. Great quantities of such high-chromium vanadium–titanium magnetite ores have not been exploited and utilized efficiently on a large scale due to the underdeveloped technology and immature utilization process. Thus, it is essential to make full use of these special iron ore deposits.

Pellets, as one vital kind of furnace burden for reduction and smelting in a blast furnace, play an important role in the ironmaking process in China. Furthermore, it is known that the principal Fe-bearing furnace burdens are pellets in North America and North Europe [10–12]. Together with sinters and lumpy ores, high-chromium vanadium–titanium magnetite pellets could be effective in the reduction and smelting in blast furnaces on a large scale, and previous researchers have conducted some exploratory work for high-chromium vanadium–titanium magnetite pellets (HCVTMP) [7,8,13]. Ou [13] studied the effect of MgO on the crushing strength, reduction, and smelting behavior of high-chromium vanadium–titanium magnetite pellets. Cheng et al. [7,8] have studied the effect of TiO_2 on the crushing strength and investigated the effect of TiO_2 and Cr_2O_3 on the reduction and smelting mechanism of high-chromium vanadium–titanium magnetite pellets. However, the effects of CaO on the basic characteristics, reduction, and smelting behavior, and the mechanism of high-chromium vanadium–titanium magnetite pellets, have been elusive.

As it is known, previous researchers have conducted some investigations on fluxed pellets [14–21]. Studies have indicated that the metallurgical properties of pellets would be improved by adding a CaO additive, although an increase in reduction swelling may occur in the finished oxidized pellets [17–20]. On one hand, previous researchers have made some detailed studies on the effects of CaO on the swelling of hematite/magnetite agglomerates and iron oxide compacts [17,18]. On the other hand, studies have been conducted on the pellet preparation from mixed hematite-magnetite concentrates, and it has been shown that adding magnetite into hematite pellets not only enables lowering the preheating and roasting temperature, but also improves the strength of preheated and roasted pellets. Thus, it is rewarding to investigate the effects of this special kind of magnetite on the crushing strength. Meanwhile, the blank of the HCVTM pellet preparation and properties can be filled in. In addition, CaO effects on the crushing strength have been referred to in Wang et al.'s and Fan et al.'s studies [14,21], but it is of great necessity to carry out further and detailed studies, especially for these HCVTM pellets. Furthermore, for the melting-dripping properties at the elevated temperature, previous workers have made some investigations [19,20]. Wang et al. [19] have studied the effect of CaO/SiO_2 on the dripping performance of vanadium–titanium burdens, in which the CaO content in the pellets was in the range of 1.12–1.60 wt % and the mass ratios of CaO/SiO_2 for furnace burdens were 1.39–1.84, and the focus on how sintered CaO/SiO_2 changes the softening-melting-dripping characteristics. Chu et al. [20] have investigated the effect of CaO/SiO_2 on the softening-dripping properties of carbon composite iron ore hot briquettes, in which the CaO content in the pellets was 0.16–3.86 wt % and the mass ratios of CaO/SiO_2 for furnace burdens were 0.07–1.80, focusing on the softening-melting-dripping of carbon-bearing pellets. Nevertheless, the effect of CaO on the metallurgical properties, including the softening-melting-dripping performance of oxidized pellets for high-chromium vanadium–titanium magnetite, is still in need of exploration. Consequently, it is of great necessity to carry out the present work for the properties of this special kind of magnetite and CaO's effects on the reduction and smelting performance of the finished pellets.

In order to better research the utilization technology, the process of high-chromium vanadium–titanium magnetite, and to provide the theoretical and practical basis, the effect of CaO on the crushing strength of high chromium vanadium–titanium magnetite pellets was first studied, and on the basis of preparing qualified pellets, the softening-melting-dripping performance was further investigated in this work.

2. Experimental

2.1. Experimental Materials

In this study, the green HCVTMP samples were prepared by mixing the material proportion of 40 wt % HCVTM, 40 wt % magnetite a, called high-grade Oukong ore, and 20 wt % magnetite b, called low-grade Oukong ore, outside with 1 wt % bentonite (the binder of pellets) and with different wt % CaO additives of 0, 2, 4, 6 and 8. The weight percent of the bentonite and CaO additive are aimed at the total weight of HCVTM, ore a and ore b. Table 1 shows the chemical composition of HCVTM and other two iron ores which were used for pelletizing with different wt % CaO additives. The pelletizing method was as follows: First, about 4 kg of pelletizing materials were calculated, weighed, and then mixed uniformly. Second, 7 wt % water was added to the mixing materials uniformly. After 40 min the mixed materials were used for pelletizing in a balling disk with a rotation rate of 18 r/min, and 2 wt % water was added during this pelletizing process. The green HCVTM pellets were then dried for five hours in the bake oven (Gongyi Yuhua Instrument Co. Ltd., Chengdu, China) at 100 °C. The (dried) green HCVTMP were oxidatively baked in the muffle furnace (Shenyang Changcheng Industrial Electric-furnace Factory, Shenyang, China) in air. The furnace was heated from room temperature to 900 °C at a ramping rate of 10 °C/min, and then the temperature was maintained constant for 10 min and further heated to 1275 °C at 5 °C/min. After further oxidation at the temperature for 20 min, the pellets were cooled inside the furnace with the heat reduced to 900 °C, then they were taken out and cooled in air to room temperature. Such prepared oxidized pellets contained about 0.2% to 0.7% of FeO, and detailed values of FeO content are 0.66 wt %, 0.71 wt %, 0.59 wt %, 0.52 wt %, and 0.18 wt % for 0 wt %, 2 wt %, 4 wt %, 6 wt %, and 8 wt % of CaO additive, respectively.

Table 1. Chemical composition of HCVTM and other two magnetite ores used for pelletizing, wt %.

Iron Ore	TFe	FeO	CaO	SiO_2	MgO	Al_2O_3	TiO_2	V_2O_5	Cr_2O_3	S	P
HCVTM	62.45	27.29	0.21	2.69	0.71	3.20	5.05	1.032	0.58	0.16	0.02
Magnetite a	68.32	27.04	0.13	4.27	0.30	0.32	-	-	-	0.09	0.01
Magnetite b	65.02	23.90	0.17	8.35	0.19	0.05	-	-	-	0.01	0.02

2.2. Softening-Melting-Dripping Procedure

The softening-melting-dripping experiments for HCVTMP with different wt % CaO were carried out in the apparatus which has been described in previous studies, and the schematic diagram of the device is shown in Figure 1 [7,22]. Before the reduction and smelting experiments, the charging method simulated the blast furnace charging conditions. Coke, 20 mm in height, was put in the bottom of the graphite crucible (Shenyang Graphite-crucible Factory, Shenyang, China) and 500 g HCVTMP were put on the nether coke, together with coke 40 mm in height on HCVTMP. The size of the HCVTMP samples and the coke were all 10–12.5 mm. After charging, the lever of the external static load and the charged graphite crucible were put in the reduction tube, and the thermocouple was placed appropriately. In order to accurately measure the external static load during the reduction and smelting, it was necessary to hermetically seal the reduction tube bottom well to prevent the gas from leaking. Then the displacement transducer (Anshan Branch Xiang Instrument Co. Ltd., Anshan, China) was adjusted to be smoothly pressed on the lever of the external static load. The external static load can be regulated during the softening-melting-dripping experiments according to the loading extent of the furnace burden in the descending process. With the preparation work done, the definite temperature regime and reduction atmosphere in different temperature ranges shown in Table 2 were adopted until the end of the dripping [7,23]. After dripping, argon gas was adopted to prevent the reduction and smelting products, including the dripped and non-dripped melted iron and slag from oxidizing until reaching room temperature. The softening-melting-dripping performance was demonstrated with the exact indices obtained during the reduction and smelting process and with the chemical analysis, XRD pattern, and microscopic examination for the dripped and non-dripped products.

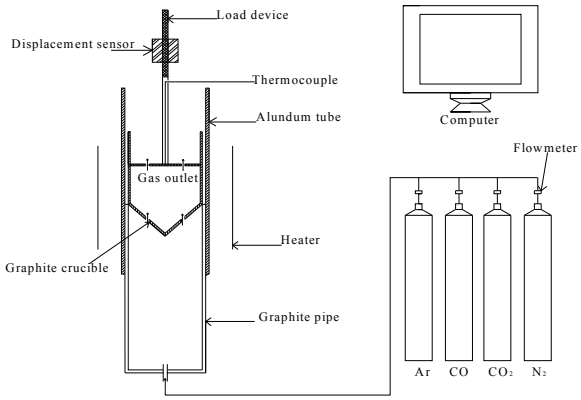

Figure 1. Schematic diagram of experimental softening-melting-dripping device.

Table 2. Temperature regime and gas atmosphere of the softening-melting-dripping experiments.

Temperature Range	0–400 °C	400–900 °C	900–1020 °C	1020 °C–Dripping Temperature
Furnace ramping rate	10 °C/min	10 °C/min	3 °C/min	5 °C/min
Gas composition	N_2 3 L/min	N_2 9 L/min CO 3.9 L/min CO_2 2.1 L/min		N_2 10.5 L/min CO 4.5 L/min

2.3. Characterization Methods

The crushing strength of HCVTMP with different CaO additives was tested with an electronic universal testing machine (EUTM, ZCQT-S50Kn; Jinan Zhongchuang Industrial Test System Co., Ltd., Jinan, China) with a maximum load of 50 kN, and the mineral phases of HCVTMP were analyzed with X-ray diffraction (XRD, X' Pert Pro; PANalytical, Almere, the Netherlands) with Cu Kα radiation at 40 kV and 40 mA (λ = 1.5406 Å). The scanned range was 2θ = 5°–90° with a step of 2θ = 0.1° and 1 s/step. The chemical compositions of both original HCVTMP samples and different reduced products, including the melted iron and slag, were analyzed by inductively-coupled plasma-atomic emission spectroscopy (ICP-AES, Optima 8300DV; PerkinElmer, Fremont, CA, USA) with a self-excited solid-state high-frequency generator at 40.68 MHz, and with X-ray fluorescence (XRF, ZSXPrimus II; Rigaku, Takatsuki, Japan) with an X-ray tube with a rhodium target at a maximum power of 4 kW (60 kV, 150 mA). The microstructures of HCVTMP, the slag, and the non-dripped products were examined with a scanning electron microscope (SEM, Ultra Plus; Carl Zeiss GmbH, Jena, Germany) with a Schottky-type field emission electron source and with resolution ratios of 0.8 nm/15 kV and 1.6 nm/1 kV at 20 V–30 kV, together with energy disperse spectroscopy (EDS, Ultra Plus; Carl Zeiss GmbH, Jena, Germany) to obtain the micro-area components. Before EUTM characterization, HCVTMP samples were the original bulks. Before XRF, ICP-AES, and XRD characterization, all of the samples were ground to fine powders. Before SEM-EDS characterization, the samples of HCVTMP, the slag, and non-dripped products were bulks.

3. Results and Discussion

3.1. Effect of CaO on the Crushing Strength of HCVTMP

The crushing strength of HCVTMP with different CaO additives that were tested with EUTM were above 2500 N/pellet, meeting the crushing strength requirements of blast furnace burdens [23,24]. The crushing strength values with 2–8 wt % CaO additives, namely 5654 N/pellet, 3873 N/pellet, 3327 N/pellet, and 2797 N/pellet, were higher than that without the CaO additive (2528 N/pellet), but the value decreased with increasing the CaO additive from 2 wt % to 8 wt %. It can be determined that the optimized mass ratio of CaO/SiO_2 was around 0.41 for the crushing strength, since the mass

ratio of CaO/SiO_2 was about 0.01 wt %, 0.41 wt %, 0.75 wt %, 1.13 wt %, and 1.44 wt % for 0 wt %, 2 wt %, 4 wt %, 6 wt %, and 8 wt % CaO additives, respectively. The mass ratios of CaO and SiO_2 were gained from the chemical analysis of oxidized HCVTMP and were referred to the original pellet preparation materials. It is well-known that suitable amounts of CaO are necessary to guarantee adequate amounts of liquid phases and slag phases in the pellets which have a relationship with the improvement of microstructures that are beneficial to increasing the pellet strength [25], and the reasoning of the crushing strength change are further elucidated with corresponding mineral phases and microstructures of HCVTMP. The XRD patterns of HCVTMP with 0 wt %, 2 wt %, 4 wt %, 6 wt %, and 8 wt % CaO additives are presented in Figure 2, in which corresponding XRD peaks of Fe_2O_3 [26], SiO_2 [27], and $Ca_3Fe_2Si_3O_{12}$ [28] were analyzed and found. Figure 3 exhibits SEM images of HCVTMP with 2, 4, and 8 wt % CaO additives at 2000×, and Figure 4 exhibits SEM image at 10,000× and EDS analyses of different areas for HCVTMP with the 2 wt % CaO additive, from which it is indicated that the pellet structure was composed of hematite phases, liquid phases of calcium iron ferrites, and slag phases of silicates. From the elemental distributions of HCVTMP with the 2 wt % CaO additive exhibited in Figure 5, it can also be observed that Si^{4+}, Al^{3+}, and Ca^{2+} were mainly distributed and dissolved in the slag and liquid phases. From XRD and SEM-EDS investigations, it is obtained that the gangue phases decreased and the slag phases of silicates and liquid phases of calcium iron ferrites increased with increasing CaO content, contributing to the increase of the crushing strength between HCVTMP without CaO additives and HCVTMP with CaO additives. When preparing pellets with certain amounts of Fe_2O_3, SiO_2, and 1–2 wt % CaO [21], the system of calcium iron ferrites was preferentially formed, and the melting point of chemical compounds and corresponding solid solutions was lower in this system. With the appearance of liquid phases, new $CaO{\cdot}SiO_2$ was generated with the reaction of SiO_2 and CaO in iron ferrites, and Fe_2O_3 was replaced and recrystallization precipitated. Thus, in the pellet structure, the predominant solid phase joining of the hematite phase recrystallization and auxiliary silicate slag phases and the connection of calcium iron ferrite among hematite phases contribute to relatively higher values of crushing strength and the stable crystal structure. The certain amounts of 2 wt % CaO in the original HCVTMP materials promoted optimized comprehensive microstructures in this study, contributing to the highest crushing strength. With increasing the CaO additive above 2 wt %, although the liquid phases in the pellet structure increased further, the bonding phenomenon of large areas occurred and considerable amounts of micro-cracks appeared owing to the pellet core shrinking and large internal stress, leading to the decrease of the crushing strength. According to above investigations, it can be concluded that the mineral phases generated during oxidative baking, and the subsequently-formed pellet microstructures, affect the crushing strength owing to the CaO addition.

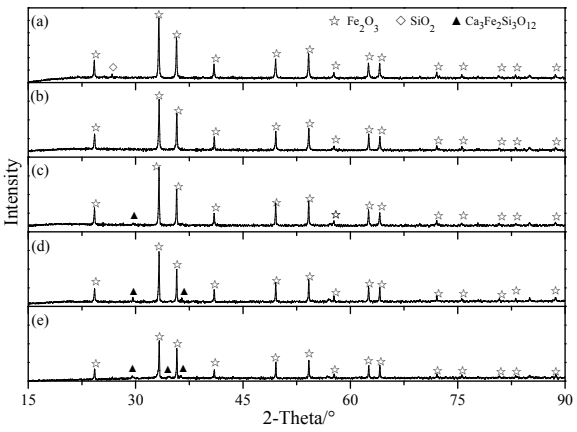

Figure 2. XRD pattern of HCVTMP with different CaO additives: (**a**) 0 wt %; (**b**) 2 wt %; (**c**) 4 wt %; (**d**) 6 wt %; and (**e**) 8 wt %.

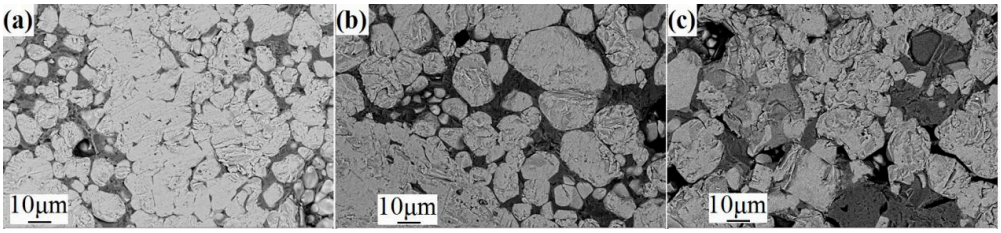

Figure 3. Scanning electron microscope (SEM) images of HCVTMP with different CaO additives at 2000×: (**a**) 2 wt %; (**b**) 4 wt %; and (**c**) 8 wt %.

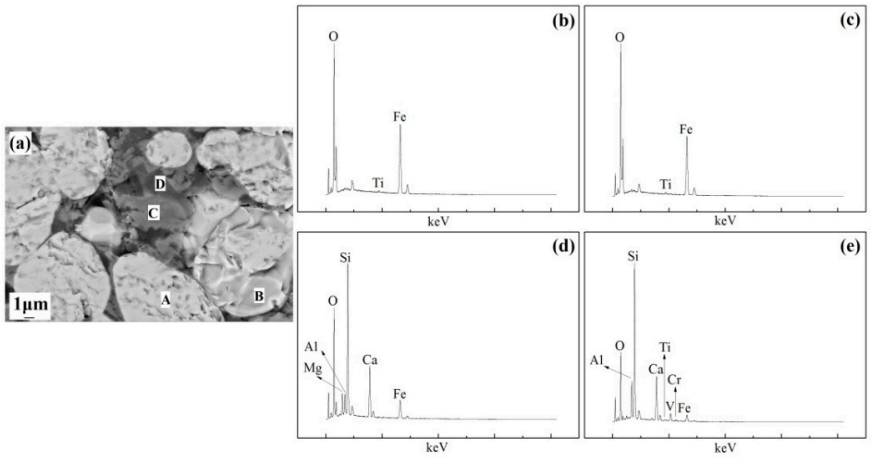

Figure 4. SEM image and energy disperse spectroscopy (EDS) analyses of different areas for HCVTMP with the 2 wt % CaO additive: (**a**) SEM image at 10,000×; (**b**) EDS analysis of area A; (**c**) EDS analysis of area B; (**d**) EDS analysis of area C; and (**e**) EDS analysis of area D.

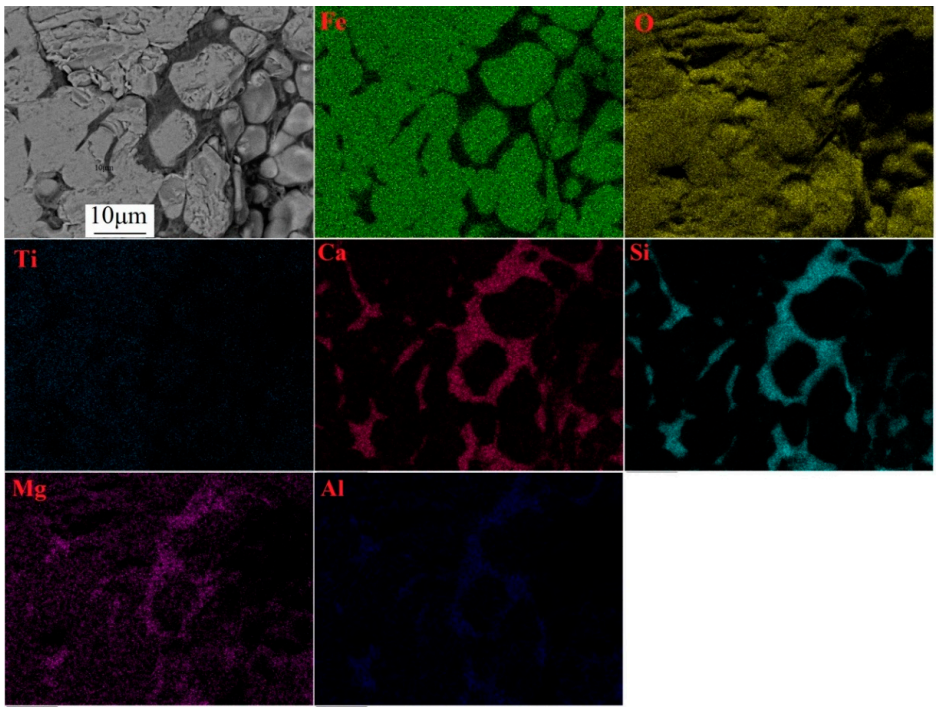

Figure 5. Elemental distributions of HCVTMP with the 2 wt % CaO additive.

3.2. Effect of CaO on the Reduction and Smelting Performance of HCVTMP

3.2.1. Softening-Melting-Dripping Behavior

In the experimental softening-melting-dripping process, accompanied by the reduction and smelting of HCVTMP furnace burdens, typical results of the external static load and contraction degree are shown in Figure 6. It is observed that the maximum external static load appeared for each furnace burden, and the melted iron began to drip from the graphite crucible after the external static load was lowered to relatively lower values of about 1451–2049 Pa. It is also found that the contraction degree was higher than 100% because the initial height was the height of the pellet burden in the graphite crucible, while the coke layer was also particularly pressed during the latter stage of the reduction and smelting process.

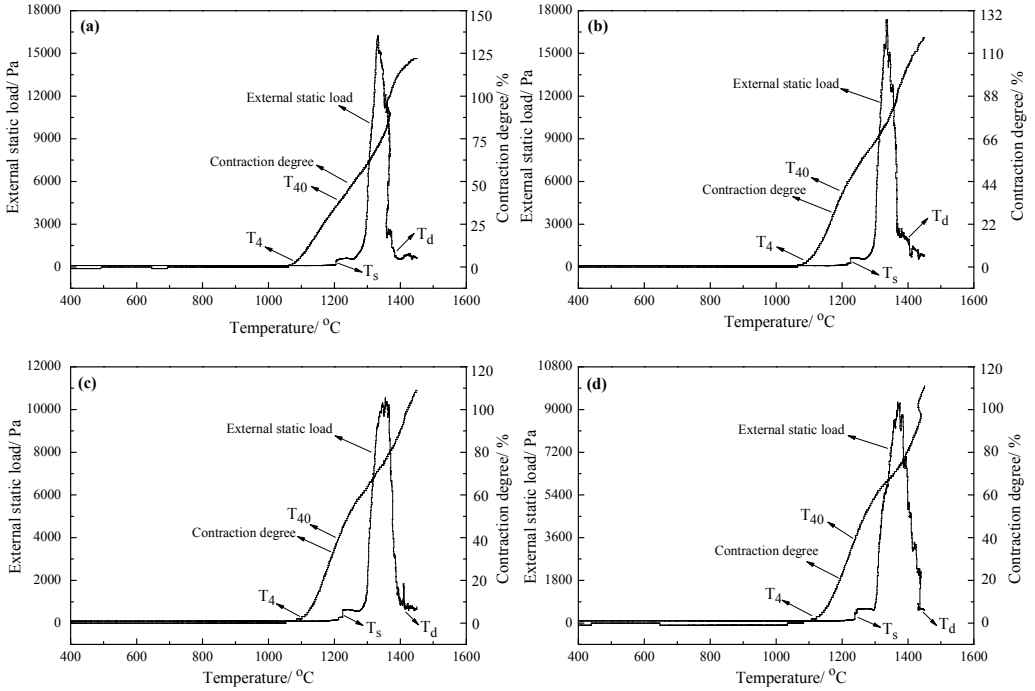

Figure 6. External static load and contraction degree for different furnace burdens of HCVTMP with CaO additives of (**a**) 2 wt %; (**b**) 4 wt %; (**c**) 6 wt %; and (**d**) 8 wt %.

Figure 7 exhibits the softening start temperature (T_4), the softening end temperature (T_{40}), and the softening zone (T_{40}–T_4) of HCVTMP. T_4 and T_{40} are the temperatures when the shrinking rate of the furnace burdens reaches 4% and 40%, respectively, during reduction and smelting, and [T_{40}–T_4] is the value of temperature difference between the softening end temperature and the softening start temperature. It is determined that the softening start temperature increased from 1088 °C to 1135 °C with the increase in the CaO additive from 0 wt % to 8 wt %, and the softening end temperature when the CaO additive was higher than that without the CaO additive. The softening end temperature decreased to 1208 °C when increasing from 2 wt % to 4 wt % first, and then increased to 1240 °C with the increase to 8 wt %. The softening zone first increased from 113 °C to 134 °C with an increase in the CaO additive from 0 wt % to 2 wt %, and then decreased to about 100 °C with an increase to 8 wt %. As it is known that the relatively higher softening start temperature and relatively narrow softening zone are beneficial to the stability of the furnace conditions and the proceeding reaction of the gas-solid reduction reaction, the increase of CaO above 2 wt % was propitious to improving the reduction and smelting index in this study. On one hand, the effect of the CaO addition on the reduction rate has a relationship with the additional proportion, temperature, and reduction

degree [29]. On the other hand, it is well-known that the softening temperature depends mainly upon the melting point of the low melting-point slag phases. With increasing CaO content, the amount of minerals with good reducibility, such as the calcium iron silicates of $Ca_3Fe_2Si_3O_{12}$ that were found in the above XRD patterns of HCVTMP, greatly increased, and the amount of titanic hematite and titanic magnetite decreased with the appearance of calcium ferrite in the process of some magnetite being oxidized into hematite [19]. Thus, the reducibility was improved with increasing CaO content, and the amount of wustite that was reduced into metallic iron increased at the same reduction condition and, correspondingly, the amount of wustite into the slag decreased, causing the melting point, the softening start temperature, and softening end temperature to increase. The reasoning of the extraordinary softening end temperature and the highest softening zone of HCVTMP with 2 wt % CaO may have a significant relationship with the slower reduction rate, owing to the optimized pellet microstructure and greater stable crystal structure.

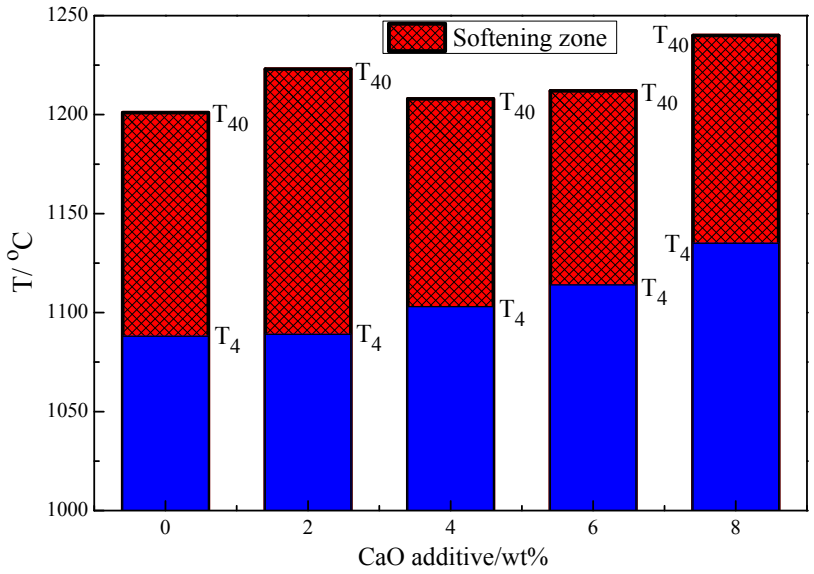

Figure 7. The effect of CaO on the softening start temperature, the softening temperature, and the softening zone of different HCVTMP furnace burdens.

Figure 8 presents the melting start temperature (T_s), the dripping temperature (T_d), and the melting-dripping zone [T_d–T_s] of HCVTMP. T_s is the temperature when the external static load promptly increased to above 400 Pa, and T_d is the temperature when the melted iron starts to drip through the graphite crucible, respectively. [T_d–T_s] is the value of the temperature difference between the dripping temperature and the melting start temperature. It is determined that the melting start temperature first underwent a decrease from 1223 °C to 1207 °C with the increase of the CaO additive from 0 wt % to 2 wt %, and then increased to 1243 °C with the increase of the CaO additive to 8 wt %. The dripping temperature increased evidently from 1338 °C to 1438 °C with the increase of the CaO additive from 0 wt % to 8 wt %, and the melting-dripping zone increased from 115 °C to 195 °C as a whole. The effect of CaO, especially with 8 wt %, has positive effects on the furnace operation by considering the melting start temperature, while the effect of CaO has negative effects on the furnace operation by considering the dripping temperature and the melting-dripping zone. There are a large number of factors influencing the melting index of the special high-chromium vanadium–titanium magnetite [7]. In addition to the influence of titanium oxides, chromium oxides, and vanadium oxides, CaO has also certain effects. With the increase of CaO content, high melting-point substances, like perovskite and schorlomite, increased in the furnace burden, contributing to the increase of the melting temperature of the furnace burdens. Furthermore, the substance of $2CaO{\cdot}SiO_2$ with the high

melting point of 2130 °C is easily formed with the existence of CaO, SiO_2, and Fe_2O_3, according to the thermodynamics calculation with Equations (1) and (2), resulting in the increase of the melting temperature with the increase in CaO content.

$$2CaO\ (s) + Fe_2O_3\ (s) = 2CaO{\cdot}Fe_2O_3\ (s),\ \Delta G^{\theta} = 53{,}100 - 2.51T\ (J{\cdot}mol^{-1}), \quad (1)$$

$$2CaO\ (s) + SiO_2\ (s) = 2CaO{\cdot}SiO_2\ (s),\ \Delta G^{\theta} = -118{,}800 - 11.3T\ (J{\cdot}mol^{-1}), \quad (2)$$

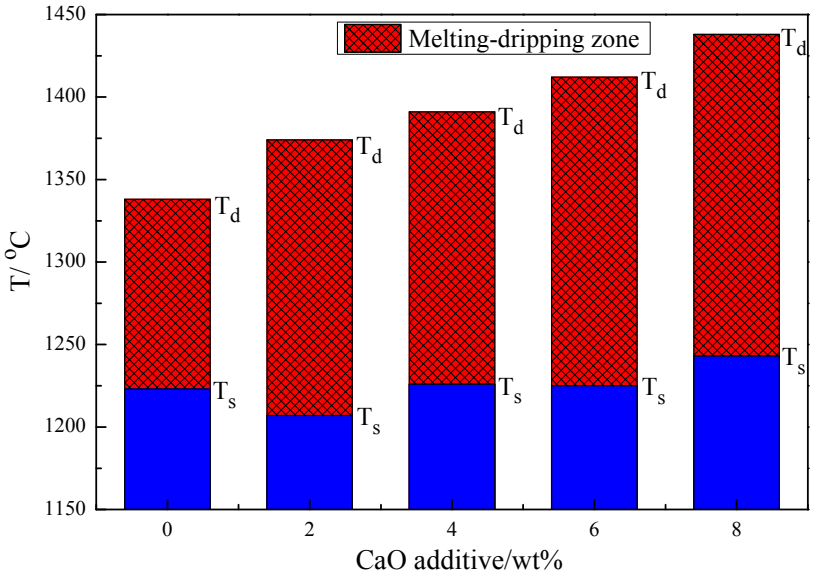

Figure 8. Effect of CaO on the melting start temperature, the dripping temperature, and the melting-dripping zone of different HCVTMP furnace burdens.

The maximum external static load and corresponding temporary temperature, external static load of dripping, and the permeability index for different furnace burdens with 0–8 wt % CaO additive are shown in Table 3. It is determined that the maximum external static load decreased from 17,722 Pa to 9311 Pa with the increase of the CaO additive from 0 wt % to 8 wt % as a whole, indicating the improvement of the gas permeability. The gas permeability index, namely the S value, was calculated according to the parameters during reduction and smelting with the equation $S = \int_{T_s}^{T_d} (\Delta P - \Delta P_s)\, dT$, which is referred to in previous studies [30,31]. ΔPs is the external static load when the temperature reached the melting start temperature and ΔP is the external static load at a different time. It is also determined that the gas permeability index decreased from 1,232,343 Pa·°C to 842,193–867,657 Pa·°C with increasing CaO content as a whole, indicating the improvement of the melting-dripping index.

Table 3. Maximum external static load and corresponding temporary temperature, external static load of dripping, and the permeability index for different furnace burdens.

CaO Additive/wt %	ΔP_{max}/Pa	$T_{\Delta P}$/°C	ΔP_d/Pa	S Value/Pa·°C
0	17,722	1291	1448	1,232,343
2	16,243	1333	2049	1,011,039
4	17,344	1337	2036	1,033,882
6	10,564	1355	1654	842,193
8	9311	1369	1451	867,657

3.2.2. Chemical Analysis

For the reduction and smelting of high-chromium vanadium–titanium magnetite pellet burdens, the separation condition of the melted iron from the slag became better and better with the increasing CaO content. It is observed that considerable amounts of the melted iron dripped from the crucible graphite and great quantities of the formed slag stayed in the crucible graphite. It is determined that the CaO additive was good at slag forming and separating from the melted iron. Table 4 presents the chemical composition analysis of the separated slag and melted iron that were analyzed by adopting ICP-AES and XRF, from which it is determined that CaO could have certain effects on the transformation behavior of Cr, V, and Ti in the formation process of the slag and melted iron with the increasing CaO additive. Cr and V contents in the melted iron increased, while Ti content in the melted iron decreased as a whole, and Cr and V contents in the slag decreased, while Ti content in the slag increased as a whole. Since CaO is beneficial to separating the melted iron and the slag, the separation index improved. For the element transformation characteristics of Cr, V, and Ti, it is further validated that the Cr and V that have been reduced to hot metal are inclined to transform to the melted iron, while Ti, which appeared as titanium oxides or generated perovskite detected in later microscopic examination, is inclined to transform to the slag. From Table 4, it can also be gained that CaO distributed in the slag increased greatly and Ca distributed in the melted iron decreased as a whole. Thus, it can be established that CaO could have a relationship with the transformation behavior of Cr, V, and Ti to some extent as determined by the predominant chemical composition analysis of ICP-AES and XRF.

Table 4. Chemical composition of the slag and melted iron, wt %.

CaO Additive/wt %	Slag							Melted Iron				
	TFe	CaO	SiO_2	CaO/SiO_2	TiO_2	V	Cr_2O_3	TFe	Ca	Ti	V	Cr
2	11.68	14.60	38.12	0.38	17.92	1.23	1.16	96.00	0.034	0.052	0.031	0.006
4	8.91	24.81	31.48	0.79	17.53	1.27	1.11	96.03	0.048	0.036	0.025	0.002
6	5.18	36.10	30.19	1.20	14.84	0.84	0.57	96.05	0.140	0.059	0.034	0.031
8	4.44	39.56	29.67	1.33	13.06	0.89	0.49	96.47	0.017	0.013	0.018	0.016

3.2.3. Microscopic Examination

Figure 9 presents SEM images of non-dripped products for HCVTMP furnace burden with 4 wt % CaO additive at 200×, 1000×, and 5000×, and Figure 10 presents corresponding EDS analyses. Additionally, with the elemental distributions of non-dripped product for the HCVTMP furnace burden with 6 wt % CaO additive exhibited in Figure 11, it is also found that Ti was not easily attached to the coke due to the CaO addition. Ti(C,N), with a high melting point, which is insoluble in the slag and melted iron, was also not detected attached to the coke. However, it has been reported that Ti(C,N) was observed to have significant dripping difficulties for different furnace burdens with different TiO_2 and Cr_2O_3 contents in previous studies [7,8]. It could be deduced that CaO addition was not only beneficial to the slag forming and separating from the melted iron, but also beneficial to the restraining of Ti(C,N), contributing to improving the melting-dripping characteristics to a large extent.

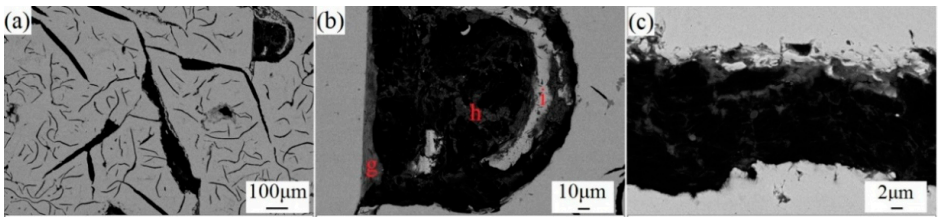

Figure 9. SEM images of non-dripped products for HCVTMP furnace burden with 4 wt % CaO additive: (**a**) at 200×; (**b**) at 1000×; and (**c**) at 5000×.

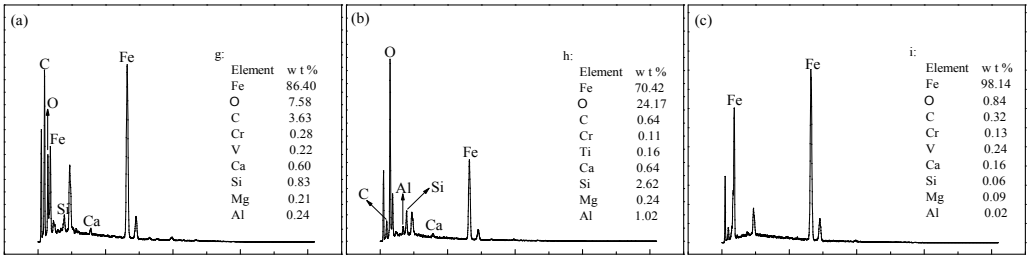

Figure 10. EDS analyses of non-dripped products for HCVTMP furnace burden with 4 wt % CaO additive: (**a**) area g; (**b**) area h; and (**c**) area i.

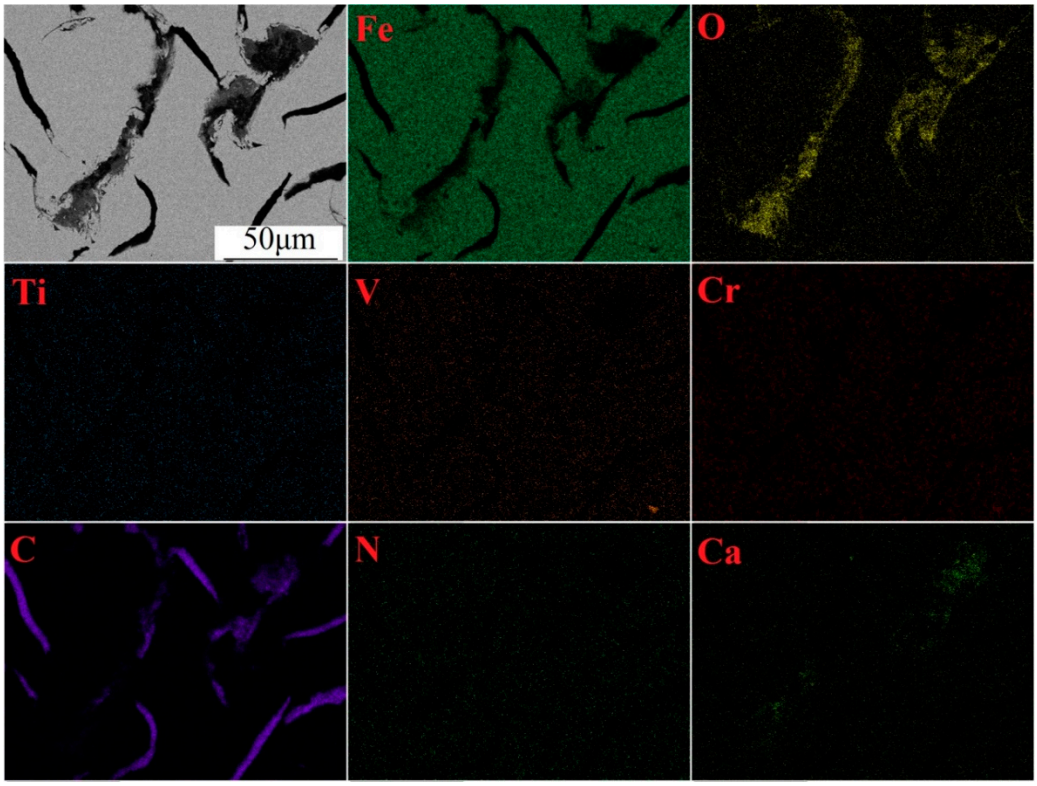

Figure 11. Elemental distributions of non-dripped product for the HCVTMP furnace burden with 6 wt % CaO additive.

The slag of the HCVTMP furnace burden with different CaO additives was further examined with the microscopic examination, with SEM images at 1000× shown in Figure 12 and the corresponding EDS analyses of areas d, e, and f presented in Figure 13. It is found that the amount of perovskite ($CaTiO_3$) increased with the increase of the CaO additive. The perovskite was detected in the slag of the furnace burden with 6 wt % and 8 wt % CaO additive, while no perovskite was found in the furnace burden with 2 wt % CaO additive. The appearance of perovskite could have a significant relationship with the melting-dripping property. On one hand, it can be calculated that $CaTiO_3$ is much more easily generated than TiC and TiN from the thermodynamic analysis with Equation (3) [3], and the appearance of $CaTiO_3$ lowered the amount of titanium carbides and titanium nitrides, contributing to improving the melting-dripping index, including the decrease of the maximum external static load and gas permeability, in accordance with above softening-melting-dripping results:

$$CaO\ (s) + TiO_2\ (s) = CaO{\cdot}TiO_2\ (s),\ \Delta G^{\theta} = -79{,}900 - 3.35T\ (J{\cdot}mol^{-1}), \quad (3)$$

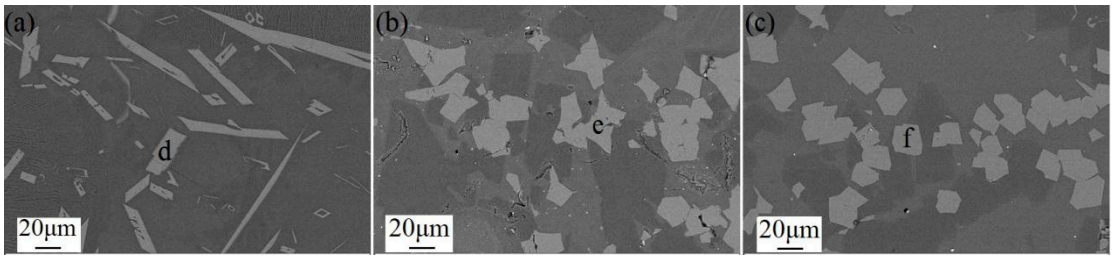

Figure 12. SEM images of slag for HCVTMP furnace burden with different CaO additives at 1000×: (**a**) 2 wt %; (**b**) 6 wt %; and (**c**) 8 wt %.

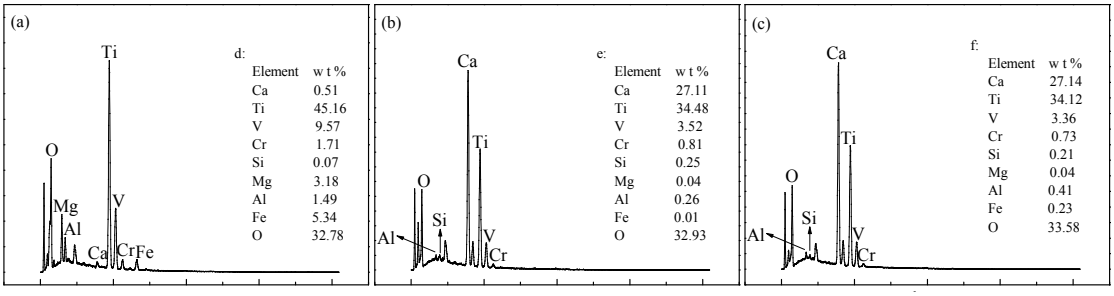

Figure 13. EDS analyses of different areas: (**a**) area d; (**b**) area e; and (**c**) area f.

On the other hand, $CaTiO_3$ has a high melting-point and is very difficult to reduce. The increase of $CaTiO_3$ resulted in the increase of the melting-dripping zone and the dripping difficulty, which was also coincident with above melting-dripping behavior.

4. Conclusions

In this work, the effect of CaO on the crushing strength, reduction, and smelting performance of high-chromium vanadium-titanium magnetite pellets was investigated, and the following conclusions can be drawn:

1. The mineral phases generated during oxidative baking, and the subsequently-formed pellet microstructures, affect the crushing strength owing to the CaO addition.
2. Although HCVTMP showed the highest crushing strength with the CaO addition of ca. 2 wt %, more CaO addition may be needed to achieve a high permeability of the furnace burdens and good separation conditions of the slag and melted iron.
3. With the predominant chemical composition analysis of ICP-AES and X-ray fluorescence (XRF), it can be determined that CaO could have a relationship with the transformation behavior of Cr, V, and Ti in the formation process of the slag and melted iron to some extent.
4. With the microscopic examination, the restraining formation of Ti(C,N) and the promoting formation of $CaTiO_3$ are in accordance with the improved melting-dripping index, including the decrease of the maximum external static load, gas permeability, and the increase of the melting-dripping zone and dripping difficulty.

Acknowledgments: The authors are especially thankful to National Project Support Program of China (Grant NO. 2015BAB19B02) and 973 Program (Grant NO. 2013CB632603).

Author Contributions: Gongjin Cheng and Xiangxin Xue conceived and designed the experiments; Gongjin Cheng and Zixian Gao performed the experiments; Gongjin Cheng, Zixian Gao and Xiangxin Xue analyzed the data; He Yang provided sample materials and contributed to the interpretation; Gongjin Cheng and Xiangxin Xue took the lead in writing the main manuscript; all authors contributed to the final manuscript version.

Conflicts of Interest: The authors declare no conflict of interest.

References

1. Wang, X.Q. *Smelting of Vanadium-Titanium Magnetite in the Blast Furnace*; Metallurgical Industry Press: Beijing, China, 1994. (In Chinese)
2. Jena, B.C.; Dresler, W.; Reilly, I.G. Extraction of titanium, vanadium and iron from titanomagnetite deposits at pipestone lake, Manitoba, Canada. *Miner. Eng.* **1995**, *8*, 159–168. [CrossRef]
3. Du, H.G. *Principle of Smelting Vanadium-Titanium Magnetite in the Blast Furnace*; Science Press: Beijing, China, 1996. (In Chinese)
4. Chen, D.S.; Song, B.; Wang, L.N.; Qi, T.; Wang, Y.; Wang, W.J. Solid state reduction of Panzhihua titanomagnetite concentrates with pulverized coal. *Miner. Eng.* **2011**, *24*, 864–869. [CrossRef]
5. Lv, X.W.; Lun, Z.G.; Yin, J.Q.; Bai, C.G. Carbothermic reduction of vanadium titanomagnetite by microwave irradiation and smelting behavior. *ISIJ Int.* **2013**, *53*, 1115–1119. [CrossRef]
6. Cheng, G.J.; Liu, J.X.; Liu, Z.G.; Chu, M.S.; Xue, X.X. Non-isothermal reduction kinetics and mechanism of high chromium vanadium–titanium magnetite pellets. *Ironmak. Steelmak.* **2015**, *42*, 17–26. [CrossRef]
7. Cheng, G.J.; Xue, X.X.; Jiang, T.; Duan, P.N. Effect of TiO_2 on the crushing strength and smelting mechanism of high chromium vanadium–titanium magnetite pellets. *Metall. Mater. Trans. B* **2016**, *47*, 1713–1726. [CrossRef]
8. Cheng, G.J.; Xue, X.X.; Gao, Z.X.; Jiang, T.; Yang, H.; Duan, P.N. Effect of Cr_2O_3 on the reduction and smelting mechanism of high-chromium vanadium-titanium magnetite pellets. *ISIJ Int.* **2016**, *56*, 1938–1947. [CrossRef]
9. He, Z.W.; Liu, J.X.; Yang, S.T.; Yang, H.; Xue, X.X. Partition of valuable components between slag and metal in the blast furnace operating with high chromium, vanadium, titanium, magnetite ores. *Metall. Res. Technol.* **2016**, *113*, 607. [CrossRef]
10. Biswas, A.K. *Principles of Blast Furnace Ironmaking—Theory and Practice*; Cootha Publishing House: Brisbane, Australia, 1981.
11. Chun, T.J.; Zhu, D.Q.; Pan, J. Influence of sulfur content in raw materials on oxidized pellets. *J. Cent. South Univ. Technol.* **2011**, *18*, 1924–1929. [CrossRef]
12. Gao, Q.J.; Shen, Y.S.; Wei, G.; Jiang, X.; Shen, F.M. Diffusion behavior and distribution regulation of MgO in MgO-bearing pellets. *Int. J. Miner. Metall. Mater.* **2016**, *23*, 1011–1018. [CrossRef]
13. Ou, H.Z. Experimental Study on Reasonable Burden Structure of Blast Furnace for Smelting Imported High Chromium Vanadium-Titanium Magnetite. Master's Thesis, Northeastern University, Shenyang, China, 2012.
14. Fan, X.H.; Gan, M.; Jiang, T.; Yuan, L.S.; Chen, X.L. Influence of flux additives on iron ore oxidized pellets. *J. Cent. South Univ. Technol.* **2010**, *17*, 732–737. [CrossRef]
15. Firth, A.R.; Garden, J.F.; Douglas, J.D. Phase equilibria and slag formation in the magnetite core of fluxed iron ore pellets. *ISIJ Int.* **2008**, *48*, 1485–1492. [CrossRef]
16. Lee, Y.S.; Ri, D.W.; Yi, S.H.; Sohn, I. Relationship between the reduction degree and strength of DRI pellets produced from iron and carbon bearing wastes using an RHF simulator. *ISIJ Int.* **2012**, *52*, 1454–1462. [CrossRef]
17. Li, G.H.; Tang, Z.K.; Zhang, Y.B.; Cui, Z.X.; Jiang, T. Reduction swelling behavior of hematite/magnetite agglomerates with addition of MgO and CaO. *Ironmak. Steelmak.* **2010**, *37*, 393–397. [CrossRef]
18. Wang, H.T.; Sohn, H.Y. Effect of CaO and SiO_2 on swelling and iron whisker formation during reduction of iron oxide compact. *Ironmak. Steelmak.* **2011**, *38*, 447–452. [CrossRef]
19. Wang, F.J.; Lv, Q.; Chen, S.J.; Liu, R.; Li, F.M. Research on influence of basicity on dropping performance of vanadium–titanium burden. *Iron Steel Vanadium Titan.* **2015**, *36*, 92–96.
20. Chu, M.S.; Liu, Z.G.; Wang, Z.C.; Fu, L.; Li, Z.N. Effects of basicity on softening-dripping properties of carbon composite iron ore hot briquette. *Iron Steel* **2010**, *45*, 9–12.
21. Wang, Z.C.; Chu, M.S.; Tang, J.; Xue, X.X. Effects of reducing atmosphere and gangue composition on reduction swelling of oxidized pellets. *J. Northeast. Univ. Nat. Sci.* **2012**, *33*, 94–97, 102.
22. Liu, J.X.; Cheng, G.J.; Liu, Z.G.; Chu, M.S.; Xue, X.X. Reduction process of pellet containing high chromic vanadium–titanium magnetite in cohesive zone. *Steel Res. Int.* **2015**, *86*, 808–816. [CrossRef]
23. Chu, M.S. *Raw Fuels and Auxiliary Materials in Ferrous Metallurgy*; Metallurgical Industry Press: Beijing, China, 2010. (In Chinese)
24. Zhang, Y.M. *Production Technology of Pellets*; Metallurgical Industry Press: Beijing, China, 2005. (In Chinese)

25. Chen, Y.M.; Chen, R. *Microstructure of Sinter and Pellet*; Central South University Press: Changsha, China, 2011. (In Chinese)
26. Yu, S.C.; Lee, J.S.; Tung, S.F.; Lan, C.L. Synthesis and structural features of a flux-grown hematite. *J. Geol. Soc. China* **1999**, *42*, 349–358.
27. Jorgensen, J.D. Compression mechanisms in α-quartz structures—SiO_2 and GeO_2. *J. Appl. Phys.* **1978**, *49*, 5473–5478. [CrossRef]
28. Novak, G.A.; Gibbs, G.V. The crystal chemistry of the silicate garnets. *Am. Mineral.* **1971**, *56*, 791–825.
29. El-Geassy, A.A. Reduction of CaO and/or MgO-doped Fe_2O_3 compacts with carbon-monoxide at 1173–1473 K. *ISIJ Int.* **1996**, *36*, 1344–1353. [CrossRef]
30. Gan, Q.; He, M.G.; He, Q. Effect of low Si and high basicity on the metallurgical properties of vanadium–titanium sinters. In Proceedings of the Ironmaking Production Technology Conference and Ironmaking Academic Convention Nationwide in 2010, Beijing, China, 26–28 May 2010; pp. 329–333, 338.
31. Liu, Z.G.; Chu, M.S.; Wang, H.T.; Zhao, W.; Xue, X.X. Effect of MgO content in sinter on the softening-melting behavior of mixed burden made from chromium-bearing vanadium–titanium magnetite. *Int. J. Miner. Metall. Mater.* **2016**, *23*, 25–32. [CrossRef]